Toxicology Reports 13 (2024) 101788

Contents lists available at ScienceDirect

Toxicology Reports

journal homepage: www.elsevier.com/locate/toxrep

Computational and theoretical insights into the cytotoxic prospects of compounds isolated from *Elaeodendron buchananii* against Leukemia

Ochuko L. Erukainure [a,*], Jennifer Nambooze [b], Chika I. Chukwuma [c], Alhadji Malloum [b,d], Aimen Aljoundi [e,f], Ghazi Elamin [g]

[a] Laser Research Centre, Faculty of Health Sciences, University of Johannesburg, Doornfontein 2028, South Africa
[b] Department of Chemistry, School of Natural Sciences, Faculty of Agriculture and Natural Science, University of the Free State, Bloemfontein 9300, South Africa
[c] Center for Quality of Health and Living, Faculty of Health Sciences, Central University of Technology, Bloemfontein 9301, South Africa
[d] Department of Physics, Faculty of Science, The University of Maroua, Maroua, Cameroon
[e] Department of Medicinal Chemistry, Collage of Pharmacy, Attahadi University, Tripoli V567-7M8, Libyan Arab Jamahiriya
[f] Department of Medicinal Chemistry, Faculty of Pharmacy, University of Tripoli, Tripoli, Libyan Arab Jamahiriya
[g] Department of Anaesthesiology & Critical Care, Nelson R Mandela School of Medicine, University of KwaZulu-Natal, Durban, South Africa

ARTICLE INFO

Keywords:
Anticancer
Computation
Cytotoxicity
Elaeodendron buchananii
And Lukemia

ABSTRACT

The present study investigated the cytotoxic prospects of isolated compounds from *Elaeodendron buchananii* against leukemia, using computational tools. Comprehensive literature searches revealed only buchaninoside, mutangin, methyl 3β-acetoxy-11α, 19α, 28-trihydroxyurs-12-en-23-oic acid, 3β, 11α, 19α-trihydroxyurs-12-en-23, 28-dioic acid, 3β-acetoxy-19α, 24, 28-trihydroxyurs-12-ene, 3-oxo-19α,28-dihydroxyurs-12-en-24-oic acid, and elabunin have been isolated from *E. buchananii*. The compounds were subjected to Density Functional Theory (DFT) and Molecular Dynamics (MD) analyses, with Fms-like tyrosine kinase (FLT3) and catalytic binding sites of Murine Leukemia Virus (MLV) as the target proteins in lukemia. Following DFT analysis, the structures of the compounds were optimized at the PW6B95D3/Def2-TZVP level of theory; their UV-Visible peaks were in the UV region, with mutangin, 3-oxo-19α,28-dihydroxyurs-12-en-24-oic acid and elabunin exhibiting one single peak. The potent Root-Mean-Square Deviation, Root-Mean-Square Fluctuation, solvent-accessible surface area and radius of gyration values indicated a strong and stable molecular interaction between the compounds and the proteins. These were further supported by high ΔG values, with MLV showing the best interaction. Per-residue decomposition plots also revealed high energy contributions in the interactions' binding sites residues. These results indicate that the cytotoxic prospects of the isolated compounds against leukemia as indicated by its molecular interactions with FLT3 and MLV.

1. Introduction

With 437,033 incident instances of cancer and 309,006 cancer-related fatalities in 2018, leukemia ranks as the fifteenth most often diagnosed cancer globally and the 11th main cause of cancer mortality, according to GLOBOCAN. Worldwide, men are more likely than women to be affected by leukemia [1]. Male age-standardized incidence rates in 2018 were 6.1 per 100,000, while female age-standardized incidence rates were 4.3 per 100,000. Male mortality was similarly greater than female mortality (2.8 per 100,000) at 4.2 per 100,000 [2]. Leukemia is expected to cause 3.1 % of new cases of cancer and 3.9 % of all cancer-related fatalities in 2024, according to the Surveillance, Epidemiology, and End Results (SEER) program [3,4]. Chronic leukemia has a typically single-modal distribution according to age, with prevalence rates that tend to rise with age. Bimodal age distributions are thus observed in ALL and acute myeloid leukemia (AML), two significant pediatric illnesses. According to GBD estimates, there was a 26 % global rise in leukemia cases between 2005 and 2015; population growth and aging were responsible for all but 3 % of this increase [1]. The burden of leukemia is distributed geographically according to the level of growth of each nation, with age-standardized rates and fatalities being greater in countries that are more advanced [5,6]. 185 nations are categorized by the IARC in the GLOBOCAN database based on the human development index (HDI), a composite indicator of living standards, education,

* Corresponding author.
E-mail address: loreks@yahoo.co.uk (O.L. Erukainure).

https://doi.org/10.1016/j.toxrep.2024.101788
Received 8 June 2024; Received in revised form 21 August 2024; Accepted 22 October 2024
Available online 30 October 2024

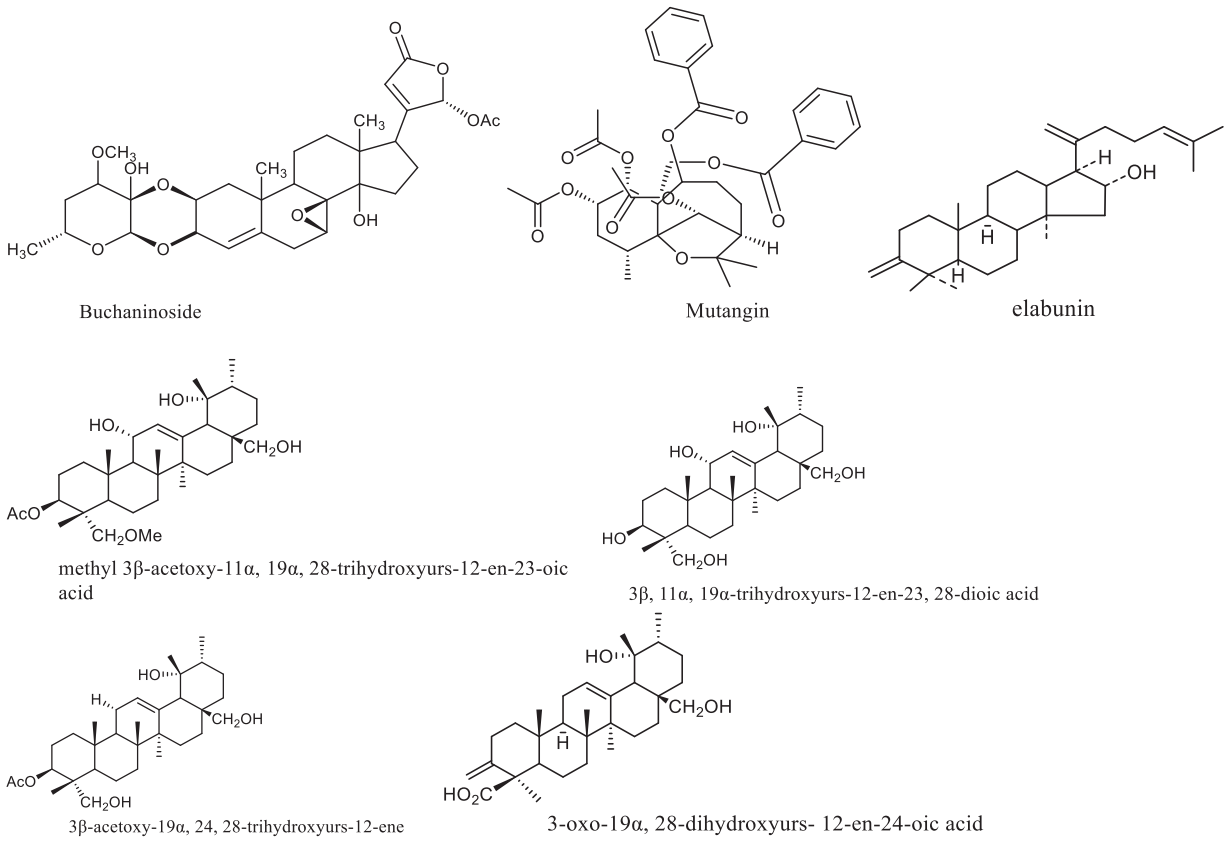

Fig. 1. Isolated compounds from *E. buchananii*.

and life expectancy. The incidence in low- and medium-income countries in 2018 was much lower in high- and very-high HDI nations (5.5 vs. 4.0 per 100,000 for men and 5.3 vs. 3.0 per 100,000 for females). According to Bray et al. [2], death rates in high/very high HDI nations and low/medium HDI countries were identical (4.5 vs. 3.2 per 100,000 for men and 2.9 vs. 2.4 per 100,000 for females).

It has long been recognized that chemotherapy and chemoprevention, blood transfusion, and haematopoietic stem cell transplantation are effective methods for managing lukemia. Inhibition of the FMS-like tyrosine kinase-3 (FLT3) ligand has been recognized as a major therapeutic mechanism of most lukemia treatments [7–9]. FLT3 is mainly expressed in the membranes of early hematopoietic progenitor cells and have been implicated in the patho-mechanism of the lukemia, with over 23 – 28 % of patients with acute myeloid lukemia (AML) reported to carry its mutations [7,9]. Targeting the murine leukemia virus (MLV) may also be a therapeutic strategy in the prevention and management of lukemia. MLV is a retrovirus belonging to the Gammaretrovirus genus and Retroviridae family [10]. It infects dividing cells only and has been implicated in the pathogensisis of several cancers including lukemia [10–12].

The main drawbacks of these therapy options are their high cost, accessibility by local population, and most crucially, their negative side effects. Therefore, these have led to the continuous search for alternative ways of treating these medical conditions, with increasing interest in traditional medicine which accounts for over 80 % of the world's basic healthcare needs because it is accessible and affordable [13].

The use of traditional herbs in the treatment and prevention of a variety of illnesses, including lukemia [14], has been practiced in traditional medicine since time immemorial. Over the years, there have been an increased interests in the use of traditional herbs as sources of natural products for the development of new drugs [15]. The development of new drugs is founded on the hypothesis that plant extracts can be used to treat several diseases. This is linked to the phytochemical constituents of these plants. Several studies have demonstrated the chemopreventive properties of these phytochemicals for a variety of cancers, including lukemia [16–18]. Among these medicinal plants with reported anticancer properties, is *Elaeodendron buchananii*.

Elaeodendron buchananii belongs to the genus *Elaeodendron* and is a member of the Celastraceae family [19]. The order Celastraceae, a suborder of the order Celastrales, contains about 96 genera and 1350 species of herbs, vines, shrubs, and small trees. Depending on the soil and temperature, *E. buchananii* can grow as a tree of different proportions in eastern Africa, primarily in Uganda, Kenya and Southern Africa like Angola, Zimbabwe, Malawi and Zambia [20]. It is an evergreen tree or shrub with a densely branching, rounded crown that can reach heights of 1–30 m. Its diameter can reach 60 cm, and its surface is frequently uneven. The tree is cut down in the wild and used locally as a source of wood and medicine [21]. According to Yelani [20], its leaf extracts are used as an oxytocic, tonic, vermifuge, abortifacient, diarrhea and fever therapy. The root decoctions are used traditionally to treat infertility, syphilis, significant uterine bleeding, coughing, and digestive problems are all treated using root decoctions [22]. The bark decoction is also used to treat diabetes, and leukemia [21,23]. These medicinal properties have been attributed to the phytochemical constituents of *E. buchananii* [24,25]. Of these phytochemicals, only seven compounds have been isolated and structurally elucidated vis-à-vis buchaninoside [19], mutangin [26], methyl 3β-acetoxy-11α, 19α, 28-trihydroxyurs-12-en-23-oic acid [25], 3β, 11α, 19α-trihydroxyurs-12-en-23, 28-dioic acid [25], 3β-acetoxy-19α, 24, 28-trihydroxyurs-12-ene [25], 3-oxo-19α,28-dihydroxyurs-12-en-24-oic acid [25], and elabunin [27].

Molecular modelling has over the years proven to be a useful tool for drug discovery. It has drawn much interests by pharmaceutical companies and research institutes owing to its low cost and reduced time in discovering new drug and their efficacies for various diseases [28]. It involves the use of computational tools such as molecular docking,

molecular dynamics, and density functional theory (DFT). Although wet lab analyses are important in determining drug efficacy and mechanism, molecular modelling can be employed as the first step in drug discovery [29].

Although their biological activities, there is still a dearth on the cytotoxic mechanism of these isolated compounds on lukemia. Thus, the present study was aimed at investigating the molecular interactions of isolated compounds from *E. buchananii* with Fms-like tyrosine kinase and catalytic binding sites of Murine leukemia virus using computational approaches.

2. Materials and methods

2.1. Compounds

The compounds of interest were those reported to be isolated from *E. buchananii*. Literature search were conducted using the academic databases – GoogleSchoolar, PubMed, and ScienceDirect. Seven compounds namely **(1)** buchaninoside, **(2)** mutangin, **(3)** methyl 3β-acetoxy-11α, 19α, 28-trihydroxyurs-12-en-23-oic acid, **(4)** 3β, 11α, 19α-trihydroxyurs-12-en-23, 28-dioic acid, **(5)** 3β-acetoxy-19α, 24, 28-trihydroxyurs-12-ene, **(6)** 3-oxo-19α,28-dihydroxyurs-12-en-24-oic acid, and **(7)** elabunin (Fig. 1) were identified and used for the present study.

2.2. Computational studies

2.2.1. Density functional theory (DFT) analysis

Initial structures of the investigated compounds were built and pre-optimized (using classical molecular dynamics with UFF force field) using the Avogadro software [30]. The structures were fully optimized using the PW6B95D3 functional of the density functional theory (DFT) [31]. The PW6B95D3 functional include the D3 dispersion corrections which are important for large sized molecules. The DFT functional was associated to the Def2-TZVP basis set for compounds not containing the actinium atom. For molecules containing the actinium atom, the DFT functional PW6B95D3 was associated to the SARC-DKH-TZVP basis set and SARC/J auxiliary basis set for the actinium atom; while the Def2-TZVP basis set was used for other atoms in the molecules. The properties of the molecules (Infrared spectrum, UV-Visible spectrum and NMR shieldings) were calculated using the same level of theory. It should be noted that, due to their computational demanding, we have not been able to compute the properties of compounds containing the actinium. However, the frequencies and their related intensities have been calculated for compounds containing the actinium atom. Some DFT-based descriptors of the studied compounds have also been calculated using the frontier molecular orbitals energies. These descriptors include the electronic gap energy, E_{gap}, (which is the difference between the energy of the HOMO, highest occupied molecular orbital, and the LUMηηO, lowest unoccupied molecular orbital), the chemical potential, μ, the chemical hardness, η, the electrophilicity index, ω, the electron affinity, EA, and the ionisation potential, IP.

$$E_{gap}=E_H-E_L \quad (1)$$

$$\mu= -(E_H+E_L)/2 \quad (2)$$

$$\eta = (E_H-E_L)/2 \quad (3)$$

$$\omega = \mu^2/2\,\eta \quad (4)$$

$$EA=-E_L \quad (5)$$

$$IP=-E_H \quad (6)$$

Where E_H and E_L are the HOMO and LUMO orbital energies, respectively.

Optimizations and properties calculation of compounds not containing the actinium atoms were performed using the Gaussian suite of program [32]. We used the *tight* option for accurate optimization. For integrals, we used the *ultrafine* grid. The optimizations and properties calculation of compounds containing the actinium atom were performed using the Orca computational chemistry program [33].

2.3. Molecular docking and molecular dynamics

2.3.1. System preparation

X-ray crystal structures of Fms-like tyrosine kinase 3 FLT3 (PDB code: 1RJB) and catalytic binding sites of Murine leukemia virus MLV (PDB code:1aol) [34,35] were attained from RSCB Protein Data Bank (PDB) [36]. To prepare these structures for molecular dynamics simulation, Molegro Molecular Viewer (MMV) [37], and UCSF Chimera software package were employed. Subsequently, Avogadro was used to optimizing the geometry of the structures and saved to be docked into the binding pockets of FLT3 and MLV [38].

2.3.2. Molecular docking and molecular dynamics simulation

Preceding docking, UCSF Chimera was used to eliminate all co-factors, non-standard residues such as Cl^-, Na^+, etc. as well as water molecules surrounding the FLT3 and Leukemia Protein structure [37]. Afterwards, the seven compounds were charged and hydrogenated. AutoDock Tools GUI was used to estimate the ligand docking and adding of a partial Gasteiger charge. Overall, system consisting of the FLT3 and MLV bound to the seven compounds underwent a 100 ns MD simulation using the AMBER18 CPU and GPU packages [39], PMEMD engine. An atomic partial charge was generated for seven ligands by means of the AMBER FF14SB of the ANTECHAMBER program [40]. The Leap module of Amber 20 enabled the addition of hydrogen atoms, sodium (Na^+), or chloride (Cl^-) counter ions to the systems for neutralization. The systems were initially minimized for 2500 steps with 500 kcal/mol $Å^2$ restraint potential, and a whole minimization step of 5000 steps was further run without restraint using the conjugate algorithm. Thereafter, the system underwent gradual heating from 0 to 300 K for 50 ps by means of a Langevin thermostat in a canonical assemblage (NVT) [41]. Following heating, equilibration was undertaken at a temperature of 300 K, excluding all restraints, and a maintained atmospheric pressure of 1 bar by utilizing the Berendsen barostat until all systems had reached equilibration [42]. The complexes then underwent a 100 ns MD simulation with the SHAKE algorithm being employed to constrict all hydrogen atoms [43]. The generated trajectories of each system were analyzed using the PTRAJ and CPPTRAJ modules [44]. The generated data and subsequent complexes were visualized using Microcal Origin analytical software [44].

2.3.3. Post-molecular dynamics simulation analysis

The bound complexes were saved after every 1 ps, and their resultant trajectories were analysed using the AMBER 20 integrated CPPTRAJ module. Post analysis for the systems MD simulation included protein, stability (RMSD), flexibility (RMSF) Radius of gyration (RoG) and solvent-accessible surface area (SASA). Binding free energy is computed by employing Molecular Mechanics/Generalized Born Surface Area (MM/GBSA) technique.

2.3.4. Binding free energy calculations

To determine an estimate of the binding free energy FLT3 and MLV bound to seven inhibitors, a method known as the Molecular Mechanics/Generalized Born Surface Area (MM/GBSA) approach, has been implemented. Binding free energy represented by ΔG_{bind} is a reliable tool that is extensively used to measure the energies that contribute to the binding of the protein and ligand to form a complex, and is calculated using the following equation:

$$\Delta G_{bind} = G_{complex} - G_{protein} - G_{inhibitor} \quad (7)$$

$$\Delta G_{bind} = E_{gas} + G_{sol} - TS \quad (8)$$

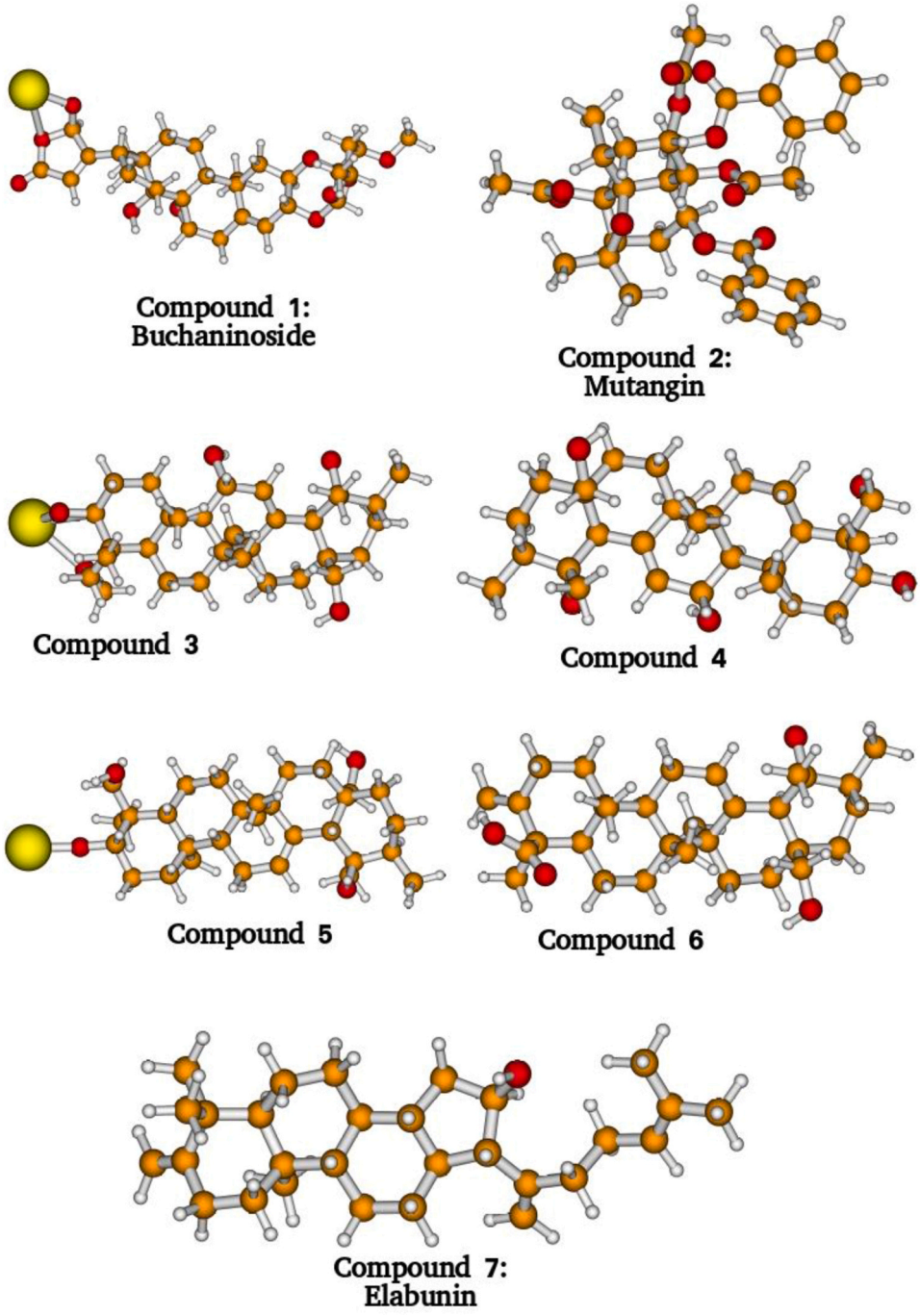

Fig. 2. Structures of the investigated compounds as optimized at the PW6B95D3/Def2-TZVP level of theory. Detailed names of the compounds are provided in the text.

Table 1
DFT-based descriptors of the studied compounds calculated at the PW6B95D3/def2-TZVP level of theory. The energy unit in the table is eV.

	E_H	E_L	Egap(eV)	μ(eV)	η(eV)	ω(eV)	EA(eV)	IP(eV)
Compound2	−7.60	−1.42	−6.18	4.51	3.09	3.29	1.42	7.60
Compound4	−6.79	−0.14	−6.65	3.47	3.32	1.81	0.14	6.79
Compound5	−3.29	−1.68	−1.61	2.48	0.81	3.83	1.68	3.29
Compound6	−6.57	−0.25	−6.32	3.41	3.16	1.84	0.25	6.57
Compound7	−6.54	0.30	−6.83	3.12	3.42	1.43	−0.30	6.54

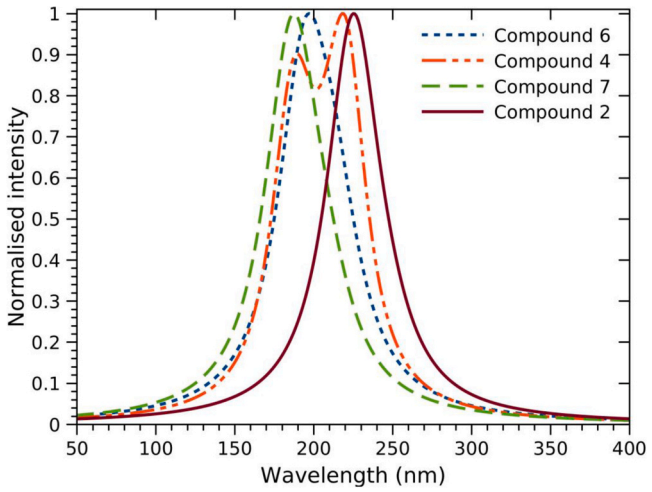

Fig. 3. UV-Vis spectra of compounds 2, 4, 6 and 7 computed using TD-DFT at the PW6B95D3/Def2-TZVP level of theory.

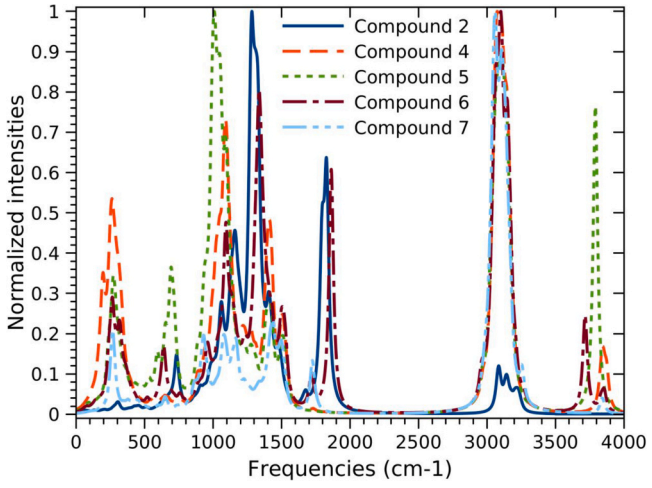

Fig. 4. Infrared spectra of the studied compounds as calculated at the PW6B95D3/Def2-TZVP level of theory.

Table 2
UV-Visible properties of the investigated compounds. We have reported the excitation energy (eV), the transition wavelength (nm), the oscillator strength associated to the strongest absorption peak, and the light harvesting efficiency (LHE).

Compounds	E(eV)	λ(eV)	fos	LHE
2	5.57	222.8	0.26	0.23
4	5.61	221.2	0.09	0.09
6	6.35	195.4	0.09	0.09
7	6.61	187.7	0.26	0.23

The ΔG_{bind} is the sum of the gas and solvent energy minus entropy (TS).

$$E_{gas} = E_{int} + E_{vdw} + E_{ele} \quad (9)$$

Where E_{gas} is representative of the addition of the internal energy terms of the AMBER force fields which includes E_{int} which represents angles, torsions, and bonds, E_{vdw} which represents covalent van der Waals energy and E_{elec} which represents the electrostatic energy components that are non-bonded.

The following equation is representative of the solvent energy calculation:

$$G_{sol} = G_{GB} + G_{SA} \quad (10)$$

$$G_{SA} = \gamma SASA \quad (11)$$

G_{GB} is representative of the polar solvation impact and G_{SA} is representative of the non-polar solvation impact which is calculated using the solvent accessible surface area (SASA). This is attained by using a water probe radius of 1.4 A°. A surface tension constant (c) was represented by a measure of 0.0072 kcal/mol and 'b' to 0 kcal/mol. The per-residue energy decomposition evaluation was also conducted to estimate the energy contribution of individual residues at the catalytic site which contributed to the stability and affinity of the compounds. This provides much atomistic insight into the inhibition demonstrated by the compounds, given that high residual energy contribution is indicative of critical residues.

Table 3
RMSD, RMSF, RoG, and SASA profile of the seven ligands when bound to FLT3.

Systems	Estimated averages (Å)			
Ligand	RMSD	RMSF	RoG	SASA
3ß, 11a, 19a-trihydroxyurs−12	1.58	1.06	19.55	14011.99
3ß-acetoxy−19a, 24, 28-trihydroxyurs	2.04	1.12	19.70	14510.63
Buchaninoside	1.34	1.03	19.45	13772.77
Elabunin	1.65	1.09	19.56	13800.19
Methyl 3ß-acetoxy−11a	1.72	1.08	19.55	13706.09
Mutangin	1.57	1.17	19.61	14271.97
3-Oxo9a,28-dihydroxyurs	1.53	1.04	19.58	14116.37

Table 4
RMSD, RMSF, RoG, and SASA profile of the seven ligands when bound to MLV.

Systems	Estimated averages (Å)			
Ligand	RMSD	RMSF	RoG	SASA
3ß, 11a, 19a-trihydroxyurs−12	1.87	1.14	18.87	11018.38
3ß-acetoxy−19a, 24, 28-trihydroxyurs	2.09	1.35	18.91	11193.50
Buchaninoside	1.80	1.06	18.80	10655.36
Elabunin	2.13	1.21	18.83	11180.05
Methyl 3ß-acetoxy−11a	2.12	1.22	18.87	11245.66
Mutangin	1.64	1.20	18.68	10948.94
3-Oxo9a,28-dihydroxyurs	1.68	1.11	18.97	11244.42

3. Results and discussion

This study employed *in silico* computational tools to investigate the preferred binding interactions of isolated compounds from *E. buchananii*. The researchers analyzed the binding of these compounds to the catalytic binding sites and individual binding pockets of two target proteins - Fms-like tyrosine kinase and Murine leukemia virus. we hypothesize that the findings from this novel molecular modelling will provide valuable guidance for understanding the design and selection of optimal inhibitor combinations. These insights could potentially lead to the development of synergistic treatment approaches targeting lukemia. Furthermore, we suggest that the outcomes of this study may open up new possibilities for combination therapy protocols against cancer in general. This study leveraged *in silico* techniques to elucidate the preferential binding properties of isolated compounds from *E. buchananii* and their interactions with key cancer-related targets. The results are expected to inform the rational design and selection of inhibitor combinations for lukemia and potentially other cancer types as well.

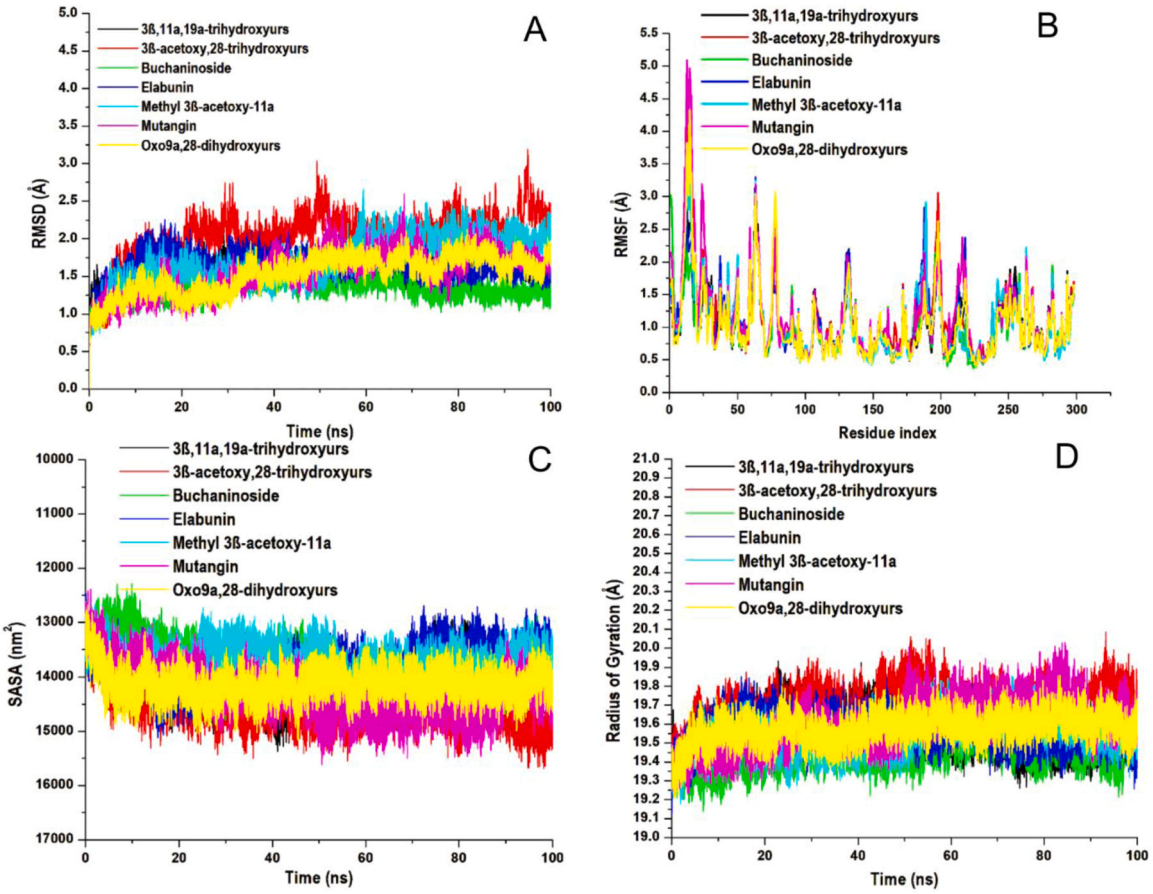

Fig. 5. Structural representation of alterations occurring during the binding of the seven compounds bound to FLT3. The (A) conformational stability, C-α atoms RMSD FLT3 to the compounds ran for 100 ns MD simulation. (B) The time evolution RMSF of each residue of the enzyme C-α atom over 100 ns for. (C) Solvent accessible surface area (SASA) backbone atoms relative to the starting minimized structure over 100 ns for FLT3. (D) C-α RoG plots and structural dynamics showing atomic distribution and compactness in various systems during 100 ns simulation period whereas the different colours represent each system atomic distribution structure conformation.

3.1. DFT analysis

3.1.1. Optimized structures of the studied compounds

Structures of the optimized compounds as optimized at the PW6B95D3/Def2-TZVP level of theory are reported in Fig. 2. Compound 1 is buchaninoside, compound 2 is mutangin, compound 3 is methyl 3β-acetoxy-11α, 19α, 28-trihydroxyurs-12-en-23-oic acid, compound 4 is 3β, 11α, 19α-trihydroxyurs-12-en-23, 28-dioic acid, compound 5 is 3β-acetoxy-19α, 24, 28-trihydroxyurs-12-ene, compound 6 is 3-oxo-19α,28-dihydroxyurs-12-en-24-oic acid, and compound 7 is elabunin.

3.1.2. DFT-based descriptors

The calculated DFT-based descriptors of the studied compounds are shown in Table 1. Examination of the gap energy shows that the actinium atom has a considerable effect on the energy gap. It was found that the compound 5 has the smallest gap energy, which indicates that the electrons can easily move from the HOMO to the LUMO. Such molecule will be highly reactive when interacting with other systems. In addition, the nucleophilicity index indicates that compound 5 is the most reactive molecule, confirming the conclusion based on the gap energy. In fact, the higher the value of the electrophilicity index, the higher the reactivity of the molecule is. Thus, compound 7 is be the less reactive molecule. This conclusion is also supported by the negative sign of the electron affinity of compound 7. A negative EA indicates that external energy is needed for the molecule to capture an extra electron. Thus, without any external energy, compound 7 will not accept any electron. Therefore, its reactivity will be reduced. Overall, the study of the DFT-based descriptors of the compounds can predict reasonably the reactivity of the studied molecules.

3.1.3. UV-Visible spectra

The UV-Visible spectra of the compounds not containing the actinium atom were calculated using the TD-DFT at the PW6B95D3/Def2-TZVP level of theory. The computed UV-Visible spectra (with intensities normalized to one) are reported in Fig. 3. To plot the spectra, the intensities are convoluted with Lorentzian profile with full with at half maximum (FWHM) of 20 nm. The results show that compounds 2, 6 and 7 exhibit one single peak while compound 4 has two distinct peaks. We have noted that all the peaks of the studied compounds are in the UV region. In addition, we have reported in Table 2, the calculated transition energy (eV), maximum wavelength (nm), oscillator strength and the light harvesting efficiency (LHE). The light harvesting efficiency (LHE) measures the optical efficiency of the studied compounds and can be calculated as: $LHE=1-e^{-fos}$, where fos is the oscillator strength associated to the maximum absorption.

3.1.4. NMR shieldings

Nuclear magnetic resonance (NRM) shielding were calculated using the GIAO approach at the PW6B95D3/Def2-TZVP level of theory. The ^{13}C and ^{1}H NMR shieldings were calculated using the tetramethylsilane (TMS) as reference molecule. The calculated chemical shielding of all the atoms of the studied molecules are reported in the supplementary material. To identify the atoms in molecules, we have provided the Cartesian coordinates of all the optimized structures in the

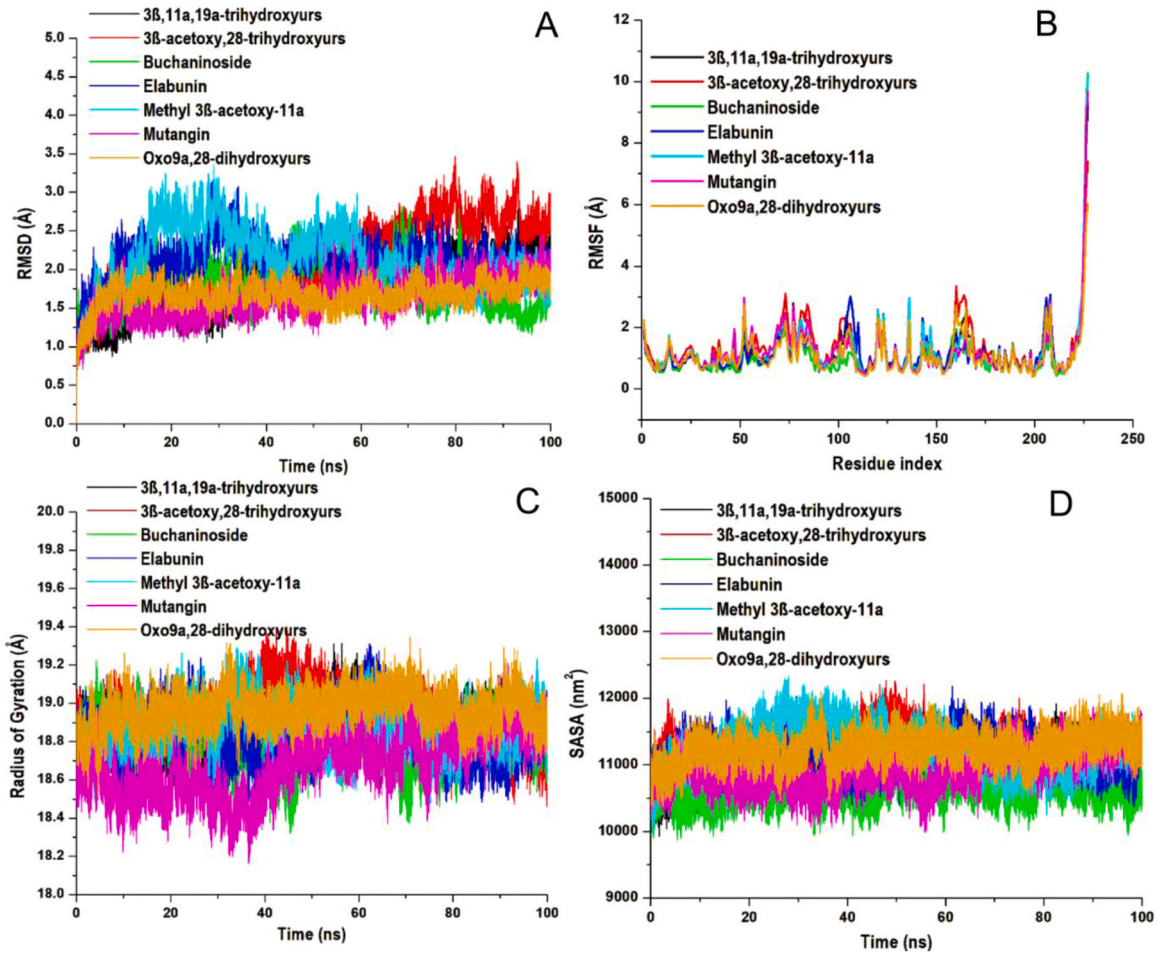

Fig. 6. Structural representation of alterations occurring during the binding of the compounds bound to MLV. The (A) conformational stability, C-α atoms RMSD MLV to the compounds ran for 100 ns MD simulation. (B) The time evolution RMSF of each residue of the enzyme C-α atom over 100 ns for. (C) Solvent accessible surface area (SASA) backbone atoms relative to the starting minimized structure over 100 ns for MLV. (D) C-α RoG plots and structural dynamics showing atomic distribution and compactness in various systems during 100 ns simulation period whereas the different colours represent each system atomic distribution structure conformation.

Table 5
MM/GBSA-based binding free energy profile of the seven ligands when bound to MLV.

Systems	Energy components (kcal/mol)				
Ligand	ΔE_{vdw}	ΔE_{ele}	ΔG_{gas}	ΔG_{sol}	ΔG_{bind}
3ß, 11a, 19a-trihydroxyurs−12	−55.87 ± 0.10	−19.57 ± 0.23	−75.44 ± 0.29	23.74 ± 0.15	−51.70 ± 0.19
3ß-acetoxy−19a, 24, 28-trihydroxyurs	−58.96 ± 0.12	−4.74 ± 0.06	−63.70 ± 0.13	13.56 ± 0.06	−50.14 ± 0.14
Buchaninoside	−31.58 ± 0.10	−37.82 ± 0.18	−69.40 ± 0.18	43.19 ± 0.14	−26.21 ± 0.09
Elabunin	−57.49 ± 0.07	−2.64 ± 0.05	−60.13 ± 0.08	6.07 ± 0.04	−54.06 ± 0.08
Methyl 3ß-acetoxy−11a	−62.34 ± 0.07	−22.13 ± 0.08	−84.47 ± 0.09	23.72 ± 0.05	−60.75 ± 0.08
Mutangin	−65.84 ± 0.11	−13.82 ± 0.11	−79.66 ± 0.15	26.37 ± 0.08	−53.29 ± 0.12
3-Oxo9a,28-dihydroxyurs	−65.27 ± 0.10	−0.45 ± 0.01	−65.72 ± 0.10	4.57 ± 0.04	−61.15 ± 0.10

All energies are in kcal/mol.
ΔE_{ele} = electrostatic energy; ΔE_{vdw} = van der Waals energy; ΔG_{bind} = total binding free energy; ΔG_{sol} = solvation free energy; ΔG_{gas} = gas phase free energy.

Table 6
MM/GBSA-based binding free energy profile of the seven ligands when bound to FLT3.

Systems	Energy components (kcal/mol)				
Ligand	ΔE_{vdw}	ΔE_{ele}	ΔG_{gas}	ΔG_{sol}	ΔG_{bind}
3ß, 11a, 19a-trihydroxyurs−12	-37.72 ± 0.07	−10.99 ± 0.11	−48.71 ± 0.12	15.95 ± 0.09	−32.76 ± 0.09
3ß-acetoxy−19a, 24, 28-trihydroxyurs	−52.04 ± 0.08	−14.84 ± 0.25	−66.88 ± 0.29	25.51 ± 0.24	−41.37 ± 0.09
Buchaninoside	−45.76 ± 0.13	−28.66 ± 0.32	−74.43 ± 0.35	35.46 ± 0.17	−38.96 ± 0.22
Elabunin	−40.85 ± 0.14	−4.45 ± 0.10	−45.30 ± 0.21	11.39 ± 0.06	−33.91 ± 0.17
Methyl 3ß-acetoxy−11a	−54.20 ± 0.09	−11.99 ± 0.11	−66.19 ± 0.11	19.40 ± 0.07	−46.79 ± 0.09
Mutangin	−33.19 ± 0.11	−12.00 ± 0.14	−45.19 ± 0.17	23.25 ± 0.13	−21.95 ± 0.08
3-Oxo9a,28-dihydroxyurs	−51.28 ± 0.06	−0.65 ± 0.01	−51.94 ± 0.07	6.27 ± 0.03	−45.67 ± 0.08

All energies are in kcal/mol.
ΔE_{ele} = electrostatic energy; ΔE_{vdw} = van der Waals energy; ΔG_{bind} = total binding free energy; ΔG_{sol} = solvation free energy; ΔG_{gas} = gas phase free energy.

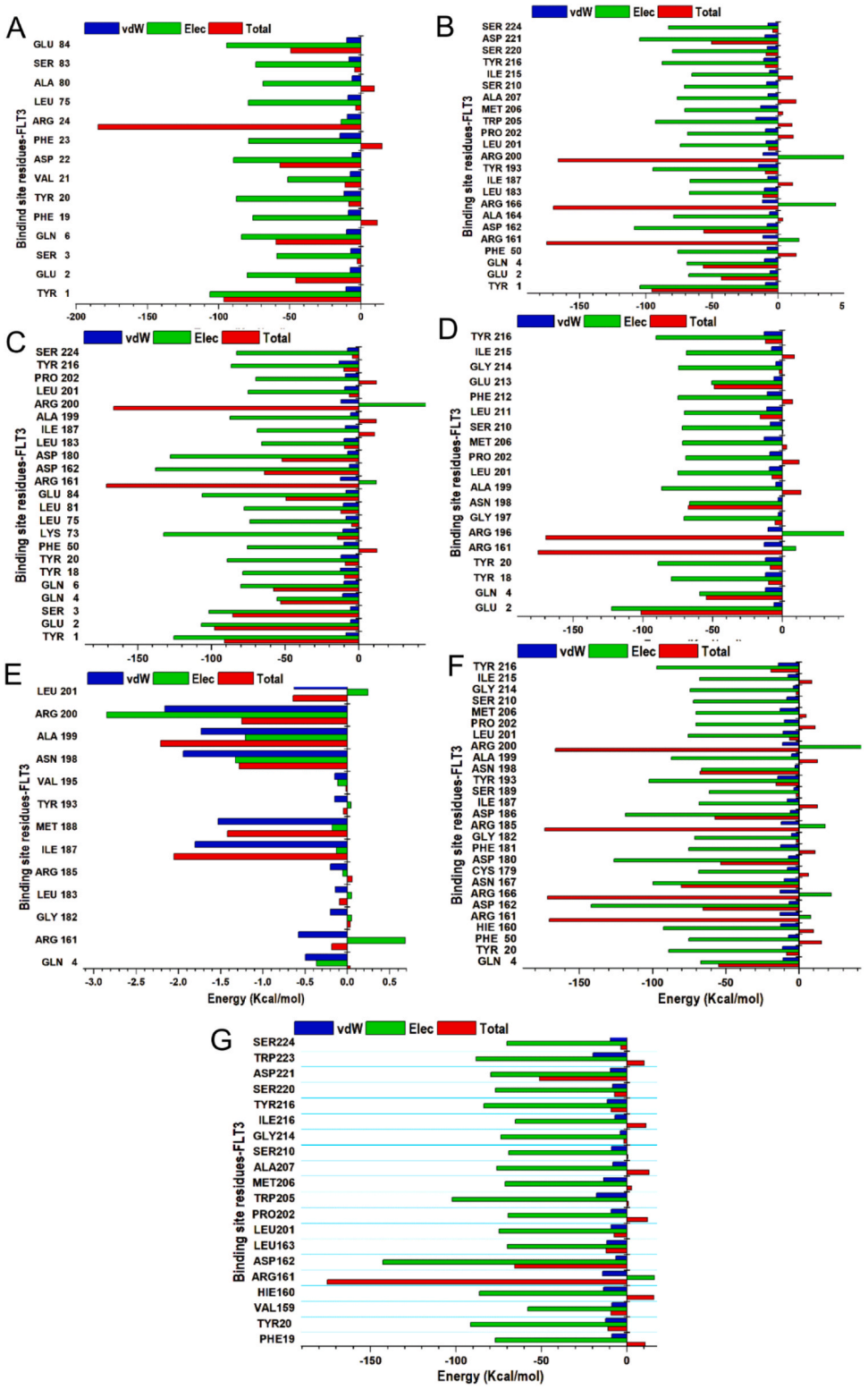

Fig. 7. Per-residue decomposition plots showing individual energy contributions to the binding and stabilization of the compounds at the binding sites of FLT3 (A) 3ß,11a,19a-trihydroxyurs (B) 3ß-acetoxy,28-trihydroxyurs (C) Buchaninoside (D) Elabunin (E) Methyl 3ß-acetoxy-11a (F) Mutangin (G) 3-Oxo9a,28-dihydroxyurs. This reveals that energy contributions were highest in binding sites residues.

supplementary material; where the atoms are following the same order as for the chemical shielding. It should be noted that, although the chemical shielding is reported for oxygen atoms these value are meaningless and should be ignore by the reader. These values have been kept just to follow the same order/position as in the Cartesian coordinates.

3.1.5. Infrared spectra of the compounds

The calculated infrared spectra of the studied compounds are reported in Fig. 3. The frequencies and their related intensities were calculated at the PW6B95D3/Def2-TZVP level of theory. To plot the infrared spectra of the studied molecules, the intensities were

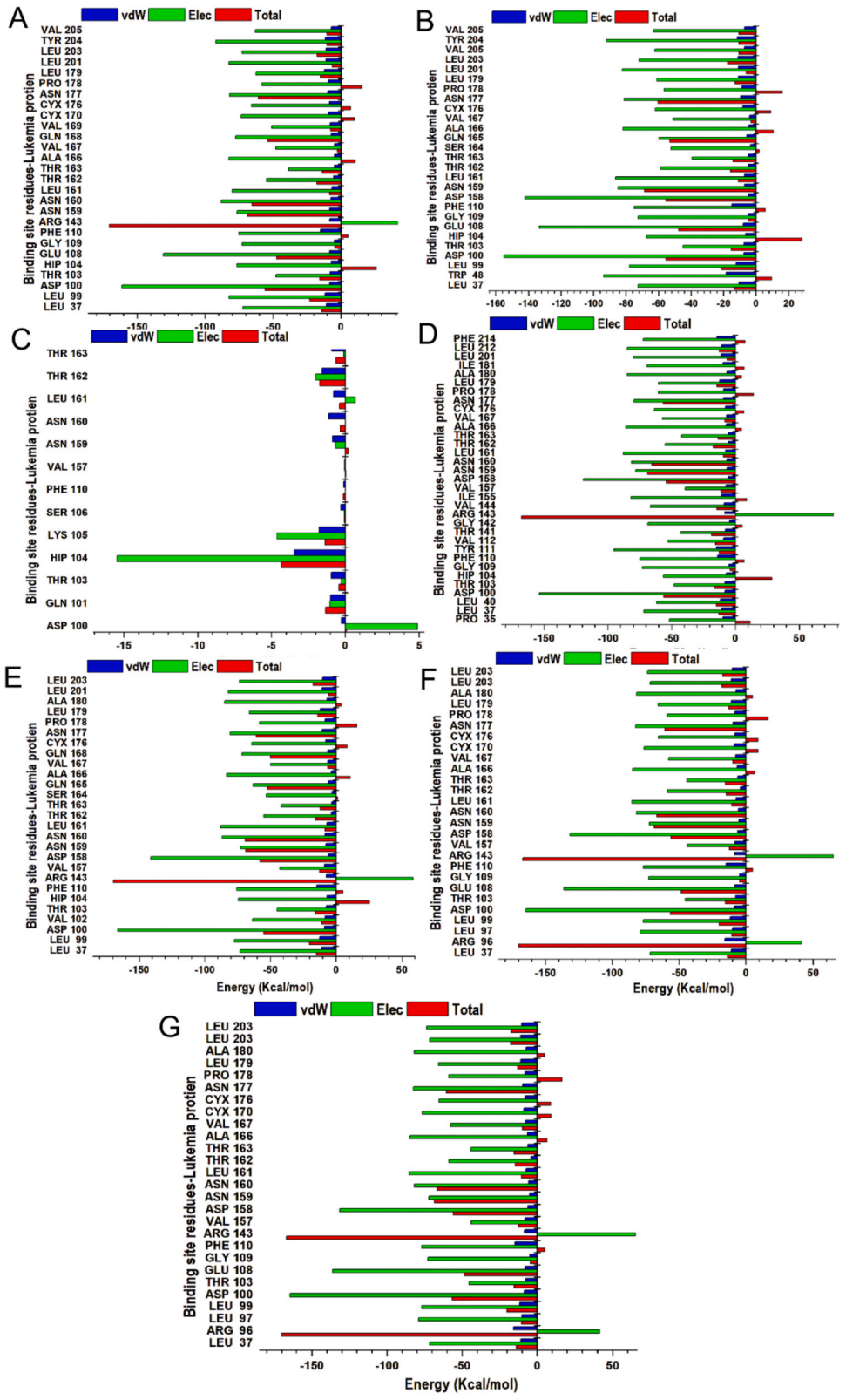

Fig. 8. Per-residue decomposition plots showing individual energy contributions to the binding and stabilization of the compounds at the binding sites of MLV (A) 3ß,11a,19a-trihydroxyurs (B) 3ß-acetoxy,28-trihydroxyurs (C) Buchaninoside (D) Elabunin (E) Methyl 3ß-acetoxy-11a (F) Mutangin (G) 3-Oxo9a,28-dihydroxyurs. This reveals that energy contributions were highest in binding sites residues.

convoluted with Lorentzian profiles with FWHM of 20 cm^{-1}.

3.2. Molecular dynamics (MD)

3.2.1. Dynamic Conformational Stability and Fluctuations

MD simulations were carried out to investigate the molecular interactions of the potential seven ligands with FLT3 and MLV targets. To validate system stability, flexibility is essential to trace disrupted motions and avoid artifacts that may arise during the course of the simulation. In this study, Root-Mean-Square Deviation (RMSD) and Root-Mean-Square Fluctuation (RMSF) was calculated to measure the systems' stability and flexibility during the 100 ns simulations. The tracing disrupted movements and preventing artifacts that could appear during the simulation need the stability of a system to be validated. Therefore, we evaluated the stability of the seven compounds inside the active sites of FLT3 and MLV. The orientation that the ligand displays within a specific binding site may have an impact on ligand stability, as the therapeutic impact of a small molecule depends on its stability in a target protein's binding region. The root mean square deviation measures the difference between a protein's backbones from its initial structural conformation to its final position. However, the residual conformational analysis is a measure of the nature of fluctuation exhibited by individual residue corresponding to the effect of ligand induction on the protein cumulatively yielding its therapeutic efficacy. For all the systems, RMSF was calculated for each amino acid residue during MD simulation of 100 ns. Moreover, the radius of gyration (RoG) is an indicator of protein compactness after ligand binding. The RoG was calculated by measuring the mass-weighted root mean square distance of the set of atoms from their shared center of mass. Furthermore, to indicate how the protein surface interrelates with solvent atoms and how it relays to the compactness of the hydrophobic protein core, the solvent-accessible surface area (SASA) of the protein upon ligand binding was calculated [45]. This was accomplished by computing the surface area of the protein observable to solvent across the 100 ns MD simulation, which is vital for biomolecular stability. According to this analysis, the average values of the compounds' RMSD, RMSF, RoG and SASA within FLT3 and MLV are presented in Tables 3 and 4. Additionally, a structural visualization using simulation RMSD, RMSF, RoG and SASA post-analyses of the compounds inside the binding site of the FLT3 and MLV are shown in Figs. 5 and 6, respectively.

3.2.2. Binding free energy landscape of the Seven inhibitors to FLT3 and MLV

The therapeutic effects elicited by a drug strongly rely on a protein's binding site and the activities that occur when binding ensues. To determine the inhibitory potential and molecular interactions of the seven compounds against the FLT3 and MLV, the binding free energy were evaluated by employing the Molecular Mechanics/Generalized Born Surface Area (MM/GBSA) method. From the results obtained, it was found that the seven compounds bound to MLV showed a higher ΔG values measuring (Table 5). Whereas, in FLT3, the bonded compounds displayed free binding energy with ΔG values lesser (Table 6). These were the highest binding energies calculated after 100 ns simulation time. Moreover, the promising ΔG values may indicate analogous modes of binding that possibly underlie the ability of these compounds to bind to these receptors.

3.2.3. Per-residue Interaction Analyses

Decompositions of the binding-free energy have been shown to present a useful insight and significant annotation of the trajectories produced by MD simulations of protein-ligand complexes. We decomposed the overall binding energy into per-residue energy contributions of individual amino acid residues in the active site to give further insight into the differences in the modes of molecular interactions of the compounds with FLT3 and MLV (Figs. 7 and 8).

Interaction between active site electropositive and electronegative residues enhances ligand binding and stabilization at the target site. This creates strong intermolecular forces of binding, which increases the binding affinity of the ligand for the active site. Furthermore, ligand-residue interactions are fundamental to the identification of key binding site residues and their corresponding interactions with the combined drugs.

Most of the amino acids showing significant critical roles of binding site residues of FLT3 and MLV were further revealed via per-residue decomposition analyses, which provided energy contributions of individual residues that interacted with ligands at the active site pockets over the 100 ns MD simulation duration as presented in Figs. 7 and 8.

4. Conclusion

Taken together, these results indicate that the cytotoxic potentials of isolated compounds from *E. buchananii* may be attributed to their molecular interactions with FLT3 and MLV, which may suggest down-regulation of these proteins and cell proliferation arrest. Thus, suggesting their prospects for the prevention and management of lukemia. However, further preclinical studies on lukemia in animal models are required to decipher these mechanism before proceeding to clinical trials.

CRediT authorship contribution statement

Ochuko L. Erukainure: Writing – original draft, Validation, Supervision, Project administration, Investigation, Formal analysis, Conceptualization. **Jennifer Nambooze:** Writing – review & editing, Resources, Investigation, Funding acquisition. **Alhadji Malloum:** Writing – original draft, Software, Methodology, Investigation. **Chika I. Chukwuma:** Writing – review & editing, Validation, Resources, Project administration, Methodology, Funding acquisition, Formal analysis. **Ghazi Elamin:** Writing – original draft, Software, Methodology, Investigation, Formal analysis. **Aimen Aljoundi:** Writing – original draft, Software, Methodology, Investigation, Formal analysis.

Declaration of Competing Interest

The authors declare that they have no known competing financial interests or personal relationships that could have appeared to influence the work reported in this paper.

Acknowledgement

JN acknowledges the Organization for Women in Science for the Developing world (OWSD) and Swedish International Development Cooperation Agency (SIDA). The authors acknowledge the National Research Foundation (NRF), Pretoria, South Africa.

Appendix A. Supporting information

Supplementary data associated with this article can be found in the online version at doi:10.1016/j.toxrep.2024.101788.

Data availability

No data was used for the research described in the article.

References

[1] J.A.B. Bispo, P.S. Pinheiro, E.K. Kobetz, Epidemiology and etiology of leukemia and lymphoma, Cold Spring Harb. Perspect. Med. 10 (6) (2020) a034819.
[2] F. Bray, J. Ferlay, I. Soerjomataram, et al., Global cancer statistics 2018: GLOBOCAN estimates of incidence and mortality worldwide for 36 cancers in 185 countries, CA: a Cancer J. Clin. 68 (6) (2018) 394–424.
[3] NCI. Cancer Stat Facts: Leukemia 2024 2023 [cited 2024 August 21]. Available from: ⟨https://seer.cancer.gov/statfacts/html/leuks.html⟩.

[4] R.L. Siegel, A.N. Giaquinto, A. Jemal, Cancer statistics, 2024, CA: a Cancer J. Clin. 74 (1) (2024).
[5] J. Huang, S.C. Chan, C.H. Ngai, et al., Disease burden, risk factors, and trends of leukaemia: a global analysis, Front. Oncol. 12 (2022) 904292.
[6] M. Du, W. Chen, K. Liu, et al., The global burden of leukemia and its attributable factors in 204 countries and territories: findings from the global burden of disease 2019 study and projections to 2030, J. Oncol. 2022 (1) (2022) 1612702.
[7] E.D. Novatcheva, Y. Anouty, I. Saunders, et al., FMS-like tyrosine kinase 3 inhibitors for the treatment of acute myeloid leukemia, Clin. Lymphoma Myeloma Leuk. 22 (3) (2022) e161–e184.
[8] Y. Zhong, R.-Z. Qiu, S.-L. Sun, et al., Small-molecule fms-like tyrosine kinase 3 inhibitors: an attractive and efficient method for the treatment of acute myeloid leukemia, J. Med. Chem. 63 (21) (2020) 12403–12428.
[9] C. Hieber, A.-H.M. Mustafa, S. Neuroth, et al., Inhibitors of the tyrosine kinases FMS-like tyrosine kinase-3 and WEE1 induce apoptosis and DNA damage synergistically in acute myeloid leukemia cells, Biomed. Pharmacother. 177 (2024) 117076.
[10] I.P. Oscorbin, M.L. Filipenko, M-MuLV reverse transcriptase: selected properties and improved mutants, Comput. Struct. Biotechnol. J. 19 (2021) 6315–6327.
[11] R. Boothpur, D.C. Brennan, Human polyoma viruses and disease with emphasis on clinical BK and JC, J. Clin. Virol. 47 (4) (2010) 306–312.
[12] C. Akkawi, J. Feuillard, F.L. Diaz, et al., Murine leukemia virus (MLV) P50 protein induces cell transformation via transcriptional regulatory function, Retrovirology 20 (1) (2023) 16.
[13] WHO. National policy on traditional medicine and regulation of herbal medicines: Report of a WHO global survey. World Health Organization; 2005.
[14] T.A. Begeno, Phytochemical investigation and characterization on the root bark extract of Prunus africana, Chem. Mater. Res. 12 (6) (2020) 8–14.
[15] R. Komakech, Y. Kang, Ethnopharmacological potential of African cherry [Prunus africana], J. Herb. Med. 17 (2019) 100283.
[16] J. Nambooze, O.L. Erukainure, C.I. Chukwuma, Phytochemistry of Prunus africana and its therapeutic effect against prostate cancer, Comp. Clin. Pathol. 31 (5) (2022) 875–893.
[17] S. Chikara, L.D. Nagaprashantha, J. Singhal, et al., Oxidative stress and dietary phytochemicals: Role in cancer chemoprevention and treatment, Cancer Lett. 413 (2018) 122–134.
[18] M. Swetha, C. Keerthana, T.P. Rayginia, et al., Cancer chemoprevention: A strategic approach using phytochemicals, Front. Pharmacol. 12 (2022) 809308.
[19] Y. Tsujino, J.I. Ogoche, H. Tazaki, et al., Buchaninoside, a steroidal glycoside from Elaeodendron buchananii, Phytochemistry 40 (3) (1995) 753–756.
[20] T. Yelani, A.A. Hussein, J.M. Meyer, Isolation and identification of poisonous triterpenoids from Elaeodendron croceum, Nat. Prod. Res. 24 (15) (2010) 1418–1425.
[21] R.H.M.J. Lemmens, in: D. Lemmens RHMJL, A.A. Oteng-Amoako (Eds.), Elaeodendron buchananii (Loes.) Loes, PROTA (Plant Resources of Tropical Africa / Ressources végétales de l'Afrique tropicale), Wageningen, Netherlands, 2010 [Internet] Record from PROTA4U.
[22] J. Nguta, J. Mbaria, D. Gakuya, et al., Antimalarial herbal remedies of Msambweni, Kenya, J. Ethnopharmacol. 128 (2) (2010) 424–432.
[23] T. Omara, A.K. Kiprop, R.C. Ramkat, et al., Medicinal plants used in traditional management of cancer in Uganda: a review of ethnobotanical surveys, phytochemistry, and anticancer studies, Evid. -Based Complement. Altern. Med. 2020 (2020) 1–26.
[24] J. Nambooze, A.P. Mishra, M. Nigam, et al., Bioactive Compounds from the Plants of the Elaeodendron Genus and Their Biological Activities—A Review, Appl. Sci. 12 (24) (2022) 12618.
[25] J.A. Odak, L.O.A. Manguro, K.-C. Wong, New compounds with antimicrobial activities from Elaeodendron buchananii stem bark, J. Asian Nat. Prod. Res. 20 (6) (2018) 510–524.
[26] M.K. Tsanuo, A. Hassanali, I.J. Jondiko, et al., Mutangin, a dihydroagarofuranoid sesquiterpene insect antifeedant from Elaeodendron buchananii, Phytochemistry 34 (3) (1993) 665–667.
[27] I. Kubo, K. Fukuhara, Elabunin, a new cytotoxic triterpene from an East African medicinal plant, Elaeodendron buchananii, J. Nat. Prod. 53 (4) (1990) 968–971.
[28] T.I. Adelusi, A.-Q.K. Oyedele, I.D. Boyenle, et al., Molecular modeling in drug discovery, Inform. Med. Unlocked 29 (2022) 100880.
[29] S.A. Hollingsworth, R.O. Dror, Molecular dynamics simulation for all, Neuron 99 (6) (2018) 1129–1143.
[30] M.D. Hanwell, D.E. Curtis, D.C. Lonie, et al., Avogadro: an advanced semantic chemical editor, visualization, and analysis platform, J. Chemin.-. 4 (1) (2012) 1–17.
[31] Y. Zhao, D.G. Truhlar, Design of density functionals that are broadly accurate for thermochemistry, thermochemical kinetics, and nonbonded interactions, J. Phys. Chem. A 109 (25) (2005) 5656–5667.
[32] Frisch MJ T.G., Schlegel H.B., Scuseria G.E., Robb M.A., Cheeseman J.R., Scalmani G., Barone V., Mennucci B., Petersson G.A. et al., Gaussian09, Revision A. Inc, Wallingford CT. 2009;121:150-166.
[33] Neese F. The ORCA program system. Wiley Interdisciplinary Reviews: Computational Molecular Science. 2012;2(1):73-78.
[34] J. Griffith, J. Black, C. Faerman, et al., The structural basis for autoinhibition of FLT3 by the juxtamembrane domain, Mol. Cell 13 (2) (2004) 169–178.
[35] D. Fass, R.A. Davey, C.A. Hamson, et al., Structure of a murine leukemia virus receptor-binding glycoprotein at 2.0 angstrom resolution, Science 277 (5332) (1997) 1662–1666.
[36] H.M. Berman, T. Battistuz, T.N. Bhat, et al., The protein data bank, Acta Crystallogr. Sect. D: Biol. Crystallogr. 58 (6) (2002) 899–907.
[37] S. Kusumaningrum, E. Budianto, S. Kosela, et al., The molecular docking of 1, 4-naphthoquinone derivatives as inhibitors of Polo-like kinase 1 using Molegro Virtual Docker, J. Appl. Pharm. Sci. 4 (11) (2014), 047-053.
[38] M.D. Hanwell, D.E. Curtis, D.C. Lonie, et al., Avogadro: an advanced semantic chemical editor, visualization, and analysis platform, J. Chemin.-. 4 (1) (2012) 17.
[39] G. Elamin, A. Aljoundi, M.E. Soliman, A synergistic multitargeted of BET and HDAC: An intra-molecular mechanism of communication in treatment of Waldenström macroglobulinemia, Mol. Simul. 48 (3) (2022) 197–208.
[40] J. Wang, R.M. Wolf, J.W. Caldwell, et al., Development and testing of a general amber force field, J. Comput. Chem. 25 (9) (2004) 1157–1174.
[41] G.S. Grest, K. Kremer, Molecular dynamics simulation for polymers in the presence of a heat bath, Phys. Rev. A 33 (5) (1986) 3628.
[42] H.J. Berendsen, Jv Postma, W.F. Van Gunsteren, et al., Molecular dynamics with coupling to an external bath, J. Chem. Phys. 81 (8) (1984) 3684–3690.
[43] J.-P. Ryckaert, G. Ciccotti, H.J. Berendsen, Numerical integration of the cartesian equations of motion of a system with constraints: molecular dynamics of n-alkanes, J. Comput. Phys. 23 (3) (1977) 327–341.
[44] D.R. Roe, Cheatham III TE. PTRAJ and CPPTRAJ: software for processing and analysis of molecular dynamics trajectory data, J. Chem. Theory Comput. 9 (7) (2013) 3084–3095.
[45] T. Zohoorian-Abootorabi, H. Sanee, H. Iranfar, et al., Separate and simultaneous binding effects through a non-cooperative behavior between cyclophosphamide hydrochloride and fluoxymesterone upon interaction with human serum albumin: Multi-spectroscopic and molecular modeling approaches, Spectrochim. Acta Part A: Mol. Biomol. Spectrosc. 88 (2012) 177–191.